AD-A052 609 TRW DEFENSE AND SPACE SYSTEMS GROUP REDONDO BEACH CALIF F/G 20/8
DEFINITION OF THE LINEAR REGION OF X-RAY INDUCED CABLE RESPONSE--ETC(U)
MAY 77 C E WULLER, L C NEILSEN, D M CLEMENT DNA001-77-C-0084
UNCLASSIFIED DNA-4405T NL

1 OF 1
AD A052609

END
DATE FILMED
5-78
DDC

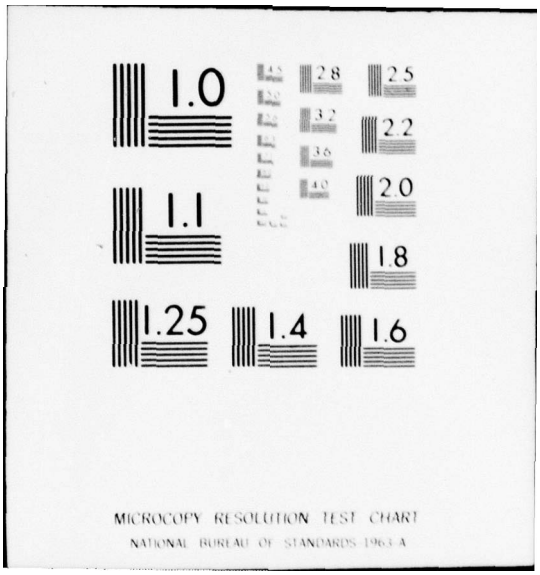
1.0
1.1
1.25
1.4
1.6
1.8
2.0
2.2
2.5
2.8
3.2
3.6
4.0
MICROCOPY RESOLUTION TEST CHART
NATIONAL BUREAU OF STANDARDS-1963-A

DNA 4405T

DEFINITION OF THE LINEAR REGION OF X-RAY INDUCED CABLE RESPONSE

TRW Defense & Space Systems Group
One Space Park
Redondo Beach, California 90278

12 ah

13 May 1977

Topical Report for Period January 1977—April 1977

CONTRACT No. DNA 001-77-C-0084

APPROVED FOR PUBLIC RELEASE;
DISTRIBUTION UNLIMITED.

THIS WORK SPONSORED BY THE DEFENSE NUCLEAR AGENCY
UNDER RDT&E RMSS CODE B323077464 R99QAXEE50307 H2590D.

Prepared for
Director
DEFENSE NUCLEAR AGENCY
Washington, D. C. 20305

Destroy this report when it is no longer needed. Do not return to sender.

UNCLASSIFIED

SECURITY CLASSIFICATION OF THIS PAGE (When Data Entered)

REPORT DOCUMENTATION PAGE

READ INSTRUCTIONS BEFORE COMPLETING FORM

1. REPORT NUMBER: DNA 4405T, AD-E300 137
2. GOVT ACCESSION NO.
3. RECIPIENT'S CATALOG NUMBER

4. TITLE (and Subtitle): DEFINITION OF THE LINEAR REGION OF X-RAY INDUCED CABLE RESPONSE.

5. TYPE OF REPORT & PERIOD COVERED: Topical Report, for Period January 1977—April 1977,
6. PERFORMING ORG. REPORT NUMBER

7. AUTHOR(s): Charles E. Wuller, L. Carlisle Neilsen, David M. Clement

8. CONTRACT OR GRANT NUMBER(s): DNA 001-77-C-0084

9. PERFORMING ORGANIZATION NAME AND ADDRESS: TRW Defense & Space Systems Group, One Space Park, Redondo Beach, California 90278

10. PROGRAM ELEMENT, PROJECT, TASK AREA & WORK UNIT NUMBERS: Subtask R99QAXE 503-07

11. CONTROLLING OFFICE NAME AND ADDRESS: Director, Defense Nuclear Agency, Washington, D.C. 20305

12. REPORT DATE: 13 May 1977
13. NUMBER OF PAGES: 26

14. MONITORING AGENCY NAME & ADDRESS (if different from Controlling Office): 24p.

15. SECURITY CLASS (of this report): UNCLASSIFIED
15a. DECLASSIFICATION/DOWNGRADING SCHEDULE

16. DISTRIBUTION STATEMENT (of this Report)

Approved for public release; distribution unlimited.

17. DISTRIBUTION STATEMENT (of the abstract entered in Block 20, if different from Report)

18. SUPPLEMENTARY NOTES

This work sponsored by the Defense Nuclear Agency under RDT&E RMSS Code B323077464 R99QAXEE50307 H2590D.

19. KEY WORDS (Continue on reverse side if necessary and identify by block number)

Cables
X-Ray Response
Linear Response
Nonlinear Response
Dielectric Conductivity
Air Conductivity
Field Limiting
Transmission Line

20. ABSTRACT (Continue on reverse side if necessary and identify by block number)

Cable response due to X-irradiation is linear with incident fluence provided the deposited charge in cable dielectrics is directly proportional to the X-ray flux. In order to estimate the level at which the linear region ends, we discuss three nonlinear processes which modify the deposited charge profile in a hypothetical cable model: field limiting in vacuum gaps, ionization effects in air gaps, and radiation-induced dielectric conductivity. The exact level, at which limiting of the Norton driver in an elemental length of cable

DD FORM 1 JAN 73 1473 EDITION OF 1 NOV 65 IS OBSOLETE

UNCLASSIFIED

SECURITY CLASSIFICATION OF THIS PAGE (When Data Entered)

409637

20. ABSTRACT (Continued)

begins, depends on the cable geometry and the X-ray source. Estimates of the onset of nonlinearities due to field limiting and to dielectric conductivity are found in terms of cable and source parameters. With air-filled gaps the Norton driver is always nonlinear. In addition to limiting of the Norton drivers, the load response of a long cable may be limited due to attenuation of propagating currents in the induced conductivity of the bulk of the dielectric.

TABLE OF CONTENTS

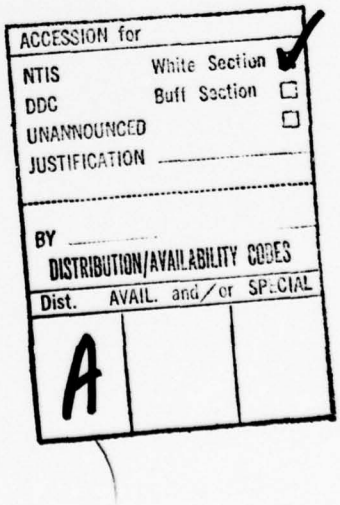

FIGURES

1. INTRODUCTION

The response of a cable to X-radiation is linear with incident photon fluence provided that the cable loads and cable impedance are non-dynamic, and the photon-electron transport is not field-limited. When these conditions do not obtain, the response is sublinear with fluence, and it is of interest to determine both the limiting effects which are responsible for this nonlinear behavior as well as the breakpoint where this limiting occurs.

The problem of determining a cable's response to X-ray photons divides naturally into three parts: (1) determine the deposition of charge in cable dielectrics (solve the electron-photon transport problem); (2) determine the induced current (solve for the Norton-equivalent drivers); and (3) determine the response of cable loads (solve the transmission line equations). The execution of the first two steps is implicit in the operation of the present generation of cable response codes.[1,2] The third step has been either simulated using a lumped element equivalent circuit[3] or solved directly, for example, by finite difference techniques.[4] The Norton drivers, which represent the input to the transmission line equations, are linear as long as the deposited charge is directly proportional to the X-ray flux. This is the case when charge transport is completely determined by the collisional stopping power of cable materials. However, as the X-ray flux increases other processes begin to modify the deposited charge profile. In this report we will discuss three of these nonlinear effects. The first two, field limiting in vacuum gaps and ionization effects in air-filled gaps, occur because gaps are commonly found in braid-shielded cables. The third effect, radiation-induced dielectric conductivity, is responsible for both limiting of the drivers and propagation losses in the cable itself. In principle, the calculation of a nonlinear driver and the solution of the transmission line problem are coupled. This is because gap effects are voltage dependent and the voltage in a given section of cable depends on the response of the entire cable including its loads, even in the case of lossless transmission lines.

The exact value of flux at which nonlinearities begin depends on the mechanism and on the particular cable's construction, e.g., gap size, dielectric material, etc. Our approach in what follows is to define a hypothetical cable with the characteristics of braid-shielded cables found in satellites or missiles and, then, to predict the short circuit current per unit length of cable as a function of flux including each limiting effect, one at a time. We will identify sensitivity parameters which affect the onset of each process. Following that we will discuss transmission lines which are simultaneously lossy and driven by nonlinear currents. The models which we present will be reduced to equivalent circuit models which can be easily evaluated using a circuit analysis computer program.

2. DEFINITION OF CABLE AND X-RAY SOURCE PARAMETERS

In this section we define a hypothetical cable as well as the X-radiation normally incident upon it. The cable is assumed to be a 50Ω coax with an inner shield radius, an outer conductor radius, and a shield gap of 0.1, .0299, and .005 cm, respectively. The conductors are copper and the dielectric is Teflon. Then, the total capacitance and inductance per unit length for the cable are 92 pF/m and 0.24 mH/m, and the propagation velocity is 0.69 c.

The X-ray environment is specified to be monoenergetic 50 keV photons whose total fluence is a parameter to be varied. We assume a triangular pulse waveform whose full-width-half-maximum is 10 ns. Holding the pulse shape constant implies fluence and flux, dose and dose rate, are proportional.

In vacuum the replacement current, or image current, tends to be proportional to the size of the gaps in the cable.[1] This is because the response is proportional to the distance the electrons emitted from each conductor travel, and since electron ranges in dielectrics are usually much less than gap sizes, the gap controls the response. Therefore, in this sample problem, we ignore charge at the center conductor/dielectric interface (where there is no gap) and take the direct injected current source to be emission from the shield which is deposited on the dielectric surface. The peak magnitude of the emission current source is taken as $1600(\mathrm{A/m})/(\mathrm{cal/cm^2})$, which is based on average emission efficiencies for copper from Dellin and MacCallum,[4] and a 10 ns pulse risetime. Then, the emission current J(t) as a function of time is

$$J = J^p f(t), \tag{1}$$

where f(t) is the envelope of the radiation pulse whose value at the peak of the pulse is unity. As a check we examine the linear short circuit current due to this source for a cable in vacuum. The emission current is weighted by the ratio of the total to gap capacitances

$$I^p_{sc} = \frac{C}{C_g} J^p = 140 \ \frac{\mathrm{A/m}}{\mathrm{cal/cm^2}} \ . \tag{2}$$

Multiplying by the pulse width of 10 ns yields a normalized response of 1.4×10^{-8} C-cm/cal, which is consistent with both analysis and experiment.[1]

3. FIELD LIMITING IN VACUUM GAPS

Consider the equivalent circuit for a section of cable given in Figure 1. The current driver J_t shown there represents transmitted charge across the shield gap which charges up the gap capacitance C_g. But the transmitted current J_t establishes a retarding electric field which opposes the motion of subsequently emitted electrons. In order to estimate the fluence at which electrons will be stopped and returned to the emitting surface, thus limiting response, we set the gap potential energy at the end of the pulse equal to the mean initial energy of created electrons $\bar{E}$,

$$e\, V_g = \bar{E}, \tag{3}$$

where e is the electronic charge. For the 50 keV X-rays assumed here, $\bar{E}$ for copper equals $\approx$ 42 keV (ref. 6). In the open circuit limit the total charge Q_t stored in the gap is equal to the integral of the emission current

$$\frac{\bar{E}}{e} = \frac{Q_t}{C_g} = \frac{F\, J^P\, \Delta t}{C_g}\ , \tag{4}$$

where F is the fluence level, and Δt is the full-width-half-maximum of the triangular pulse. Then, the onset of field limiting will occur at

$$F = \frac{\bar{E}\, C_g}{e\, J^P \Delta t} \approx 2.5\ \text{cal/cm}^2, \tag{5}$$

when evaluated using the parameters from the last section. This expression indicates that the upper bound of the linear regime decreases as the electron spectrum softens, as the gap thickness increases, and as the emission yield increases, on account of the field limiting effect.

An analytic expression for the current transmitted across the gap J_t can be obtained by starting with the Vlasov equation (the collisionless Boltzmann transport equation). Since electron transit times in a gap are short compared to typical pulse lengths, we seek a nonrelativistic steady state result dependent on the instantaneous gap voltage and on the photo-emission energy distribution. Since the circumference of a gap is much greater than its width, we approximate the system by a planar diode. Then, the electron distribution function is given by the Vlasov equation

$$v\, \frac{\partial f}{\partial x} + a\, \frac{\partial f}{\partial v} = 0, \tag{6}$$

where the deceleration due to the field build up in the gap is

$$a = \frac{-e\, V_g}{m\, d}\ , \tag{7}$$

and V_g is the magnitude of the gap potential difference, m is the electronic mass, and d is the gap width.

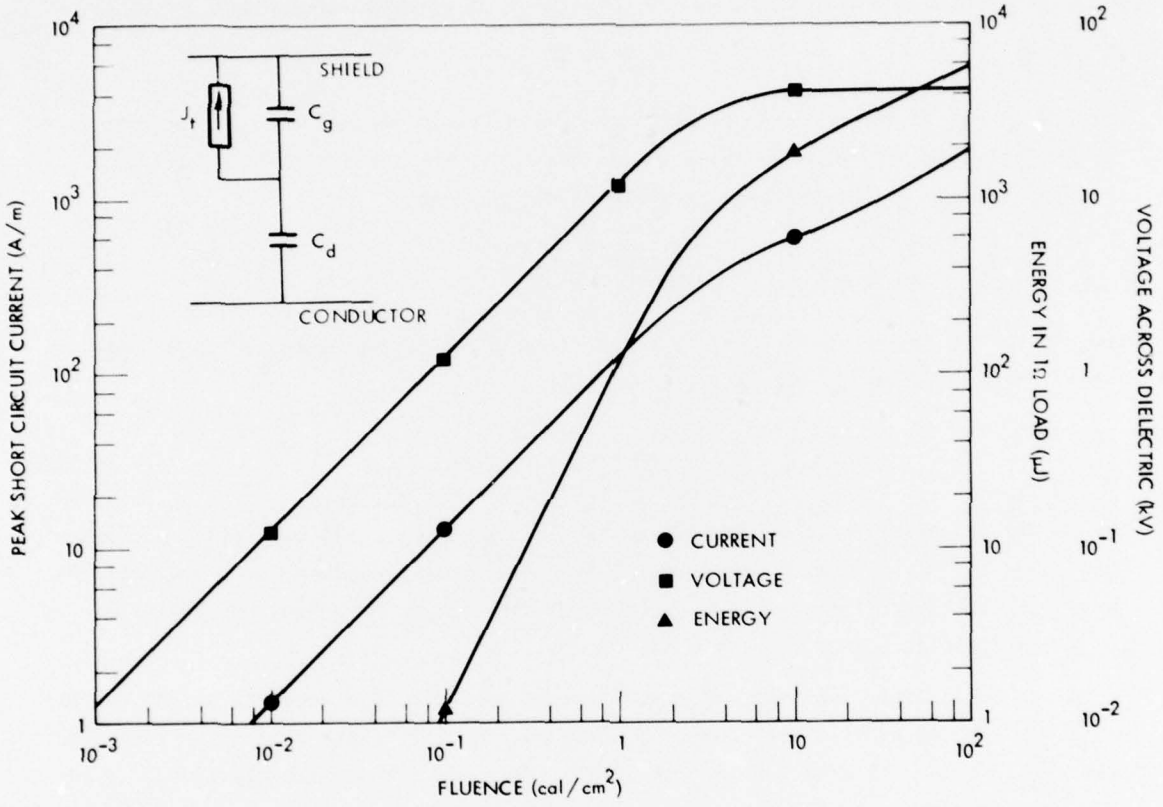

Figure 1. Response as a Function of Fluence of a Unit Section of Cable Including Field Limiting of Electron Emission into the Gap.

This ignores space charge interactions in the gap. From the theory of quasilinear partial differential equations, total energy

$$u = \frac{mv^2}{2} - \frac{ax}{m} , \tag{8}$$

is a constant of the motion in Eq. (6) and any function of u is a solution of Eq. (6). We can construct the solution for the diode region $0 \leq x \leq d$ subject to the boundary conditions that the distribution function at the emitting surface $f(x = 0, v > 0)$ is known and that all particles reaching the other side have positive velocities $f(x = d, v < 0) = 0$. The first moment of the distribution function is the transmitted current and transforming to the energy variable we get

$$J_t = J^p \, f(t) \int_{eV_g}^{\infty} n(E) \, dE, \tag{9}$$

where n(E) is the normalized energy distribution of emitted electrons.

The emission energy distribution could be found in detail from analytic transport theory or Monte Carlo calculation; however, for this illustration, we take a result from the simple X-ray induced emission theory given by Schaefer.[6] The differential energy yield at normal incidence is approximately

$$\frac{dY}{dE} = \frac{\mu_i}{4} \left(\frac{dE}{dx} \right)^{-1} , \tag{10}$$

where μ_i is the linear absorption coefficient at the incident X-ray energy for interaction with the i-th electron shell. Now it is known that the range varies roughly as E^2 for a number of materials. Thus, the stopping power and the differential energy yield should vary as E and n(E) is proportional to E. This approximately linear energy variation has been observed both in Monte Carlo calculations and experimental results. The use of a roughly linear energy spectrum appears justified as long as photon energies are not too near absorption edges and the Compton contribution is ignored. Figure 2 shows the distribution used in this calculation. We assume that the lower bound of the distribution is 1 keV.

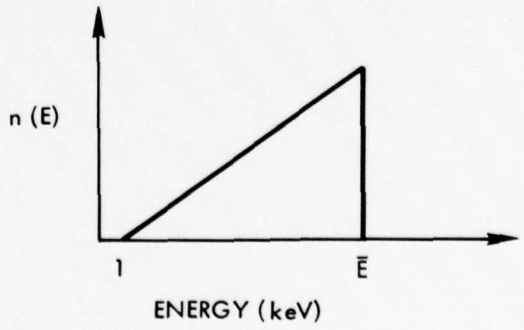

Figure 2. Assumed Differential Energy Spectrum of Electron Emission from the Cable Shield.

The peak short circuit current will be nonlinear with respect to fluence when the integral in Eq. (9) becomes less than unity. Figure 1 shows the response versus fluence of a unit section of cable driven by the field limiting source. The breakpoint between the linear and nonlinear parts of the current plot is close to the 2.5 cal/cm^2 level estimated above. The energy delivered to a 1Ω load between the shield and center conductor is also given in the figure. (One ohm is essentially a short circuit compared to the capacitive impedance.) Also plotted is the voltage built up across the dielectric layer which is equal in magnitude to the voltage across the gap because of the short circuit condition. The potential saturates at 42 kV, the voltage required to reduce the transmitted current to zero. Note that this is equivalent to an electric field of 6×10^5 V/cm in the dielectric which is more than twice the rated strength of Teflon (2.4×10^5 V/cm), although less than that of Kapton (2.8×10^6 V/cm), which is the strongest of dielectrics used in cables. This suggests that there may be combinations of environments and cable types for which dielectric breakdown could occur. Further investigations of this possibility are anticipated using our detailed cable code.

To translate the abscissa of Figure 1, and similar figures which follow, from fluence to peak flux, dose, and peak dose rate use the conversion factor 1 cal/cm^2 corresponds to 10^8 $cal/cm^2 \cdot sec$, 10^5 rad(Si), 10^{13} rad(Si)/sec.

The time history of the short circuit current is triangular and identical to the X-ray pulse shape in the linear regime. With the onset of limiting the latter part is clipped off and the pulse gets progressively narrower with increasing fluence. Figure 3 shows that the current waveform changes abruptly between 1 and 10 cal/cm^2. The triangular shape at 1 cal/cm^2 shows that response was still linear at this level.

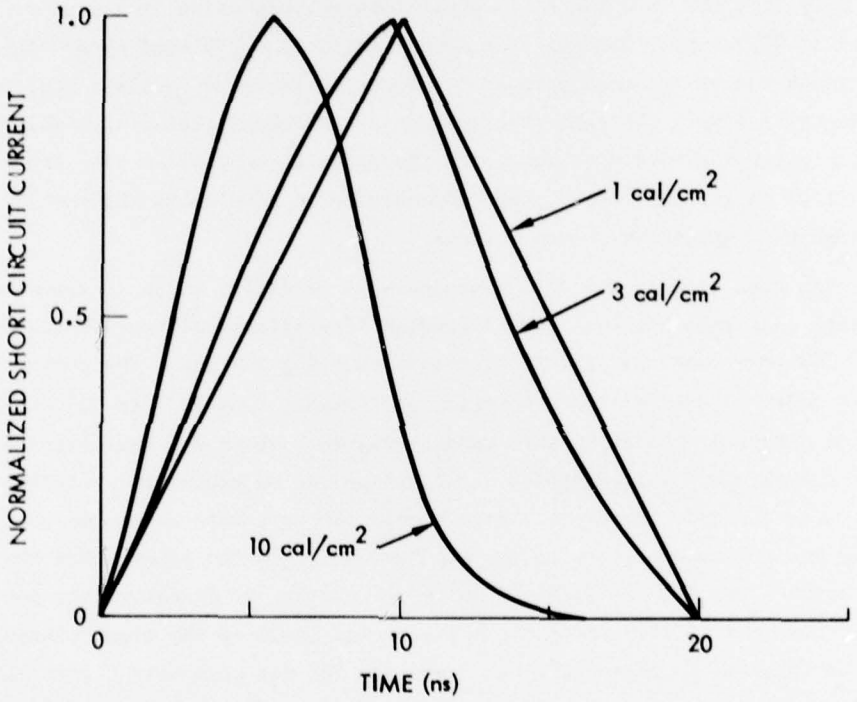

Figure 3. Comparison of Normalized Short Circuit Current Waveforms at Three Fluence Levels Showing the Effect of Field Limiting in the Gap.

4. IONIZATION EFFECTS IN AIR GAPS

When an air-filled cable gap is irradiated by X-rays, ionization of the air results in a secondary conduction current which tends to mitigate the primary photo-Compton current emitted from the metal surface. In order to include the air conductivity effect we will calculate the radiation-induced transient air conductivity of the gap and translate this into a time-dependent shunt resistance

$$R_a = \epsilon_o / C_g \, \sigma_a(t) \ , \tag{11}$$

which is then inserted into the cable equivalent circuit shown in Figure 4. Following the method of Wuller and Clement,[7] the conductivity is calculated by solving air-ion rate equations for the concentrations of secondary electrons, generic positive, and generic negative ions. The coefficients such as attachment rates, recombination rates, etc., which enter the rate equations, and the particle mobilities are functions of the electric field in the gap. Thus, the conductivity is coupled to the rest of the circuit through the instantaneous gap voltage.

The dose rate in air at 1 atmosphere of pressure, which is required in the conductivity calculations, is 1.8×10^{13} (rad(air)/sec)/(cal/cm^2) and includes energy loss contributions from the primary electrons crossing the gap. The short circuit current is shown in Figure 4 as a function of fluence, from 10^{-3} to 10^{2} cal/cm^2. The response is always nonlinear in this range. Figure 5 shows the characteristic bipolar signal of the air gap cable response. This shape can be explained as follows. The emission current source transfers charge across the gap; this continues until the electric field and the conductivity in the gap have built to the point where the secondary electron current can compete with the emission current and discharge the potential built up during the first part of the pulse, which leads to the sign reversal in the current. As fluence increases the time required for the secondary current to become comparable to the emission current decreases. This trend can be seen in the current waveforms at 10^{-3} and 10^{-1} cal/cm^2 given in Figure 5. Above 10^{-1} cal/cm^2 the current spikes are very sharp, occuring in the first few nanoseconds of the radiation pulse, and the short circuit current remains near zero for the rest of the event. Now, returning to Figure 4, the magnitudes of both peaks in the short circuit current have been plotted along with the energy which would be delivered to a 1Ω load. The dependence is sublinear with fluence throughout the range examined.

It should be pointed out that a conductivity picture of air ionization is appropriate only as long as the motion of the secondary electrons and ions is completely specified by their mobilities. At low pressures, this is no longer true, and a coupled solution of Poisson's equation and the equations of motion for particle dynamics is required. This has been considered by Wuller in one dimension (radial) for coaxial cables.[8] For a cable with a .01 cm gap the transition from air-like to vacuum-like response was found to occur near 0.1 atm.

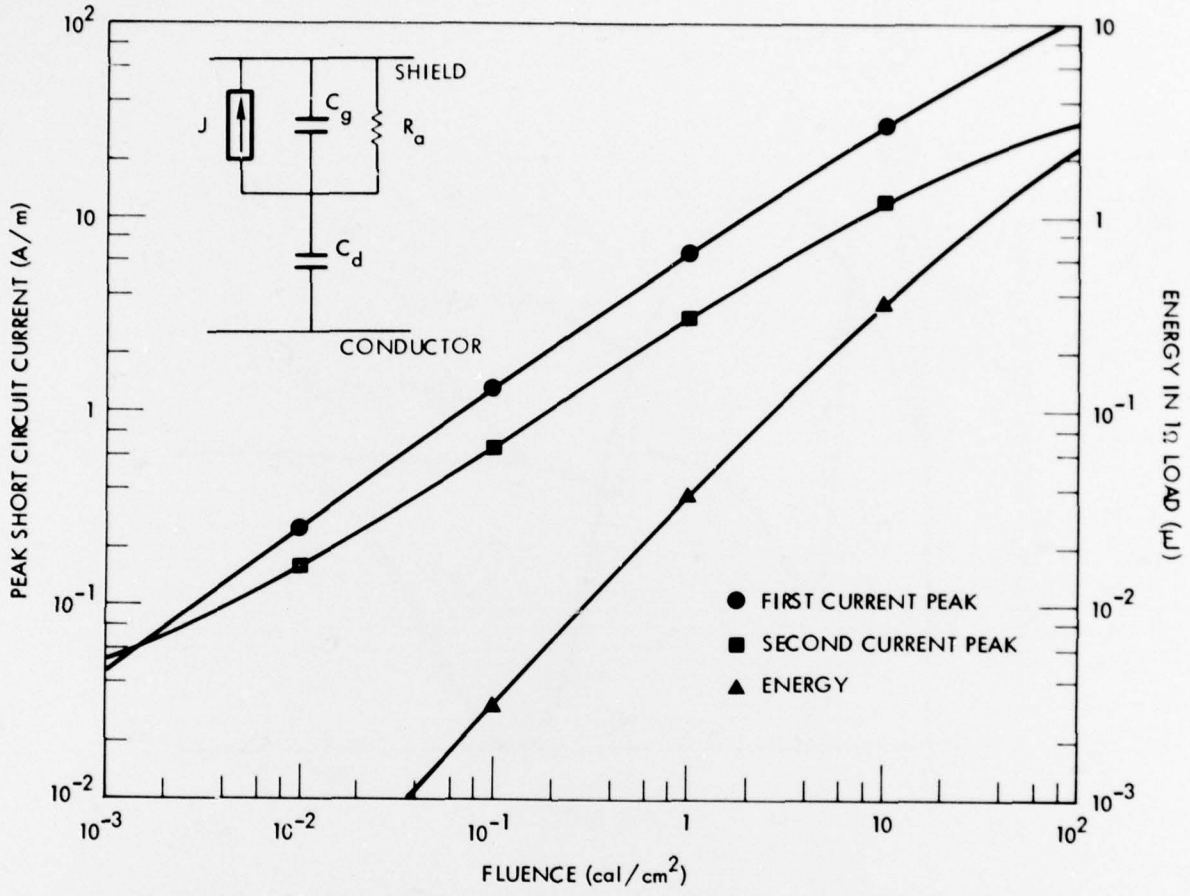

Figure 4. Response as a Function of Fluence of a Unit Section of Cable Including Transient Conductivity in the Air-Filled Gap.

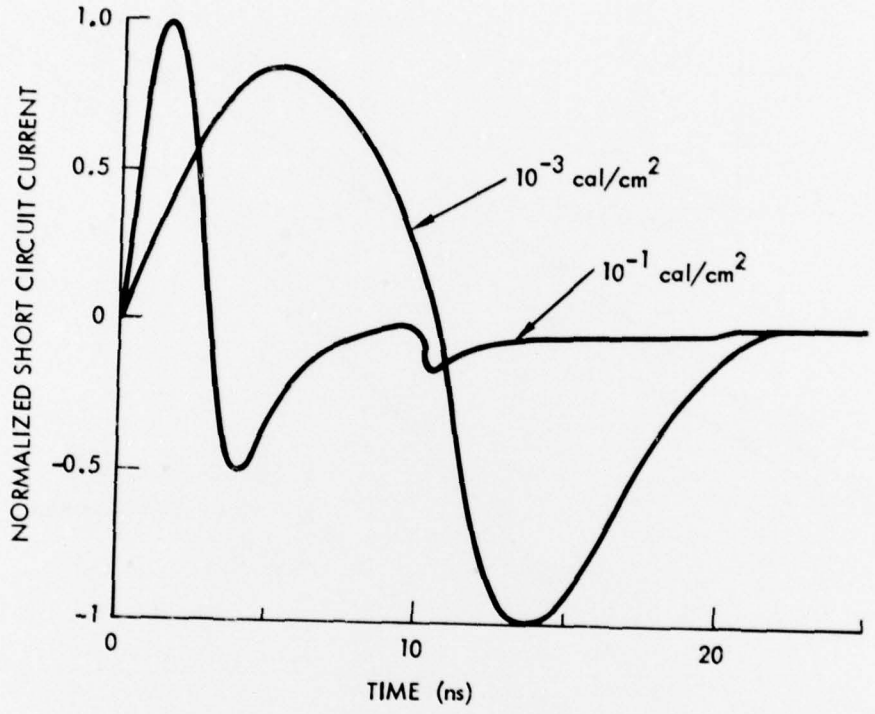

Figure 5. Comparison of Normalized Short Circuit Current Waveforms at Two Fluence Levels Showing the Effect of Ionization in an Air-filled Gap.

5. RADIATION-INDUCED DIELECTRIC CONDUCTIVITY

Ionization of the cable dielectric can have a shunting effect on the direct injection current resulting from a radiation-induced conductivity. This conductivity, in general, has prompt and delayed parts

$$\frac{\sigma(t)}{\epsilon\epsilon_o} = K_p \dot{D}^p f(t) + K_d \dot{D}^p \int_{-\infty}^{t} f(t') \exp\left[-(t-t')/\tau\right] dt' \ , \tag{12}$$

where $\dot{D}^p$ is the peak dose rate and K_p, K_d, and τ are parameters determined from short pulsed irradiations.[9] For Teflon, K_p and K_d are 1.1×10^{-5} (mho/f)/(rad/sec) and 280. (mho/f)/(rad) and τ is 216 ns. Weingart, et al,[10] and Sullivan and Ewing[11] agree on the prompt coefficient for Teflon; however, Sullivan and Ewing do not report delayed conductivity data. In the rest of this section, we assume that the transient dielectric conductivity is entirely prompt. Then, the transient resistance per length for a uniformly irradiated dielectric has the form

$$R = 1/K_p \dot{D}^p f(t)\ C \ , \tag{13}$$

where C is the capacitance per length of the cable.

In order to illustrate limiting due to dielectric conductivity alone, we revise our model cable, eliminating the gap. Assuming that the gap has been filled with Teflon, the shield emission current will penetrate one electron range ($\sim7.5\times10^{-4}$ cm for 42 keV electrons) into the dielectric. The dose rate in the bulk of the Teflon is 9.8×10^{11} (rad/sec)/(cal/cm^2). Assuming that energy is uniformly deposited by electrons stopping in the dielectric, the dose rate will be enhanced in the stopping region about a factor of 50 times the bulk dose rate. Figure 6 shows the cable equivalent circuit containing shunt resistances in the dose enhanced and bulk regions. In the short circuit case

$$V_e + V_b = 0 \ , \tag{14}$$

and the node equations for this circuit

$$I_{sc} = J + C_e \frac{dV_e}{dt} + \frac{V_e}{R_e} \ , \tag{15}$$

and

$$I_{sc} = C_b \frac{dV_b}{dt} + \frac{V_b}{R_b} \ , \tag{16}$$

can be solved for the short circuit current I_{sc}, subject to the condition that both the current source and the inverse of the resistances (conductances) have the same time history, i.e.,

$$\frac{J}{R^{-1}} = JR = \text{constant.}$$

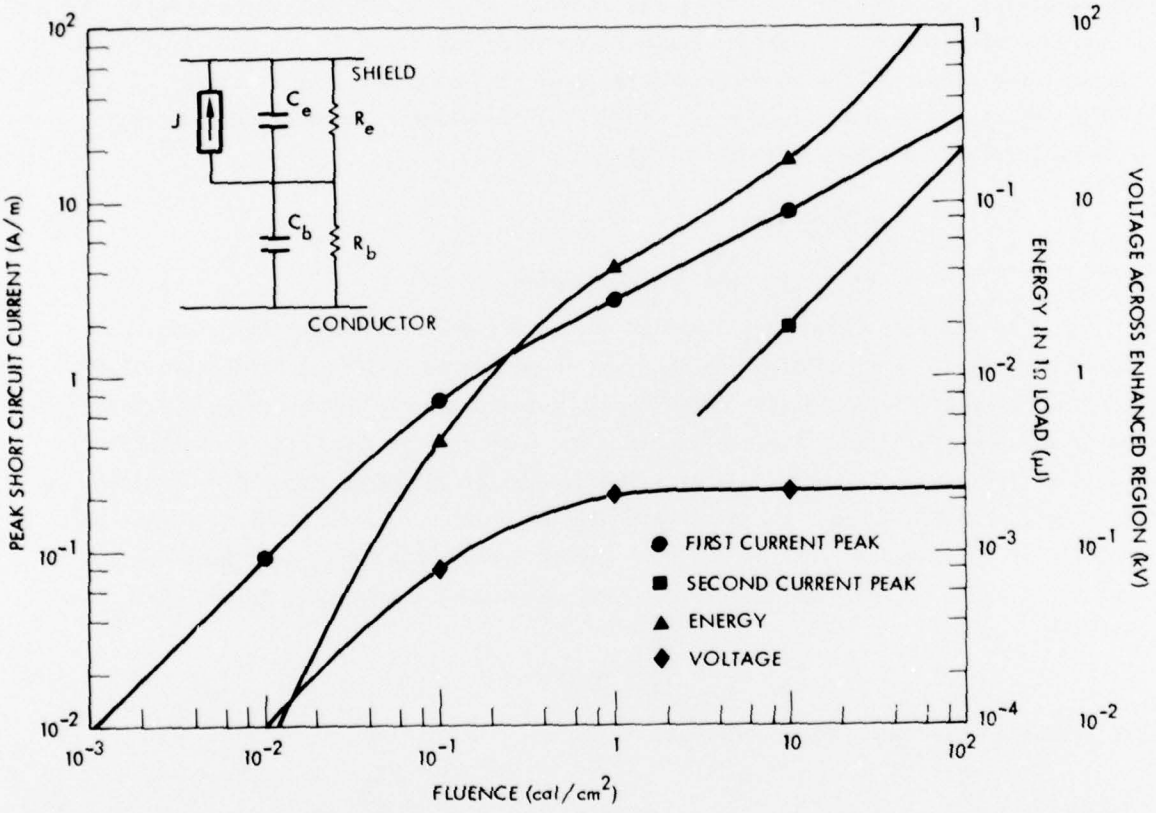

Figure 6. Response as a Function of Fluence of a Unit Section of Cable Including Transient Dielectric Conductivity in the Enhanced and Bulk Regions.

The result for the short circuit current is

$$I_{sc} = J^p f(t) \left[\frac{1}{1 + (\dot{D}^p_e C_e / \dot{D}^p_b C_b)} \right] + J^p f(t) \left[\frac{1}{1 + (C_e/C_b)} - \frac{1}{1 + (\dot{D}^p_e C_e / \dot{D}^p_b C_b)} \right] e^{\alpha}, \quad (17)$$

where

$$\alpha = - \frac{K_p (\dot{D}^p_e C_e + \dot{D}^p_b C_b)}{C_e + C_b} \int_o^t f(t') \, dt' .$$

This expression will be useful for explaining our results. Note that the first term follows the radiation pulse, while the second damps out as a function of accumulated dose.

We should see evidence of dielectric conductivity, i.e., the onset of limiting, when the discharging time of the enhanced region capacitance through its shunt resistance is comparable to the full-width-half-maximum of the X-ray pulse

$$R_e C_e \approx \Delta t . \quad (13)$$

Using Eq. (13) to evaluate R_e at the peak of the pulse, then

$$1/K_p \dot{D}^p_e = \Delta t . \quad (19)$$

Note that this dose rate $\dot{D}^p_e$ is enhanced by the factor f, such that $\dot{D}^p_e = f \dot{D}^p_b$.

Relating $\dot{D}^p_b$ to the total non-enhanced dose D via $D = \dot{D}^p_b \Delta t$, we obtain

$$D = 1/fK_p . \quad (20)$$

For Teflon this corresponds to 10^5 rads (Teflon) or 0.2 cal/cm^2 incident.

Figure 6 shows our data for the response of the cable section obtained by evaluating the equivalent circuit over a range of fluences. Above 2 cal/cm^2 we have plotted the magnitudes of both current peaks which are visible in the current waveforms. Figure 7 compares the current waveforms at several fluence levels. From the linear (triangular) shape at 10^{-2} cal/cm^2 the current peak narrows and moves away from the peak of the photon pulse. The second term of Eq. (17) dominates the waveform except at very high fluence (10 cal/cm^2), when it appears as an initial spike on top of the term proportional to the X-ray pulse shape. Returning to Figure 6, note that the break between the linear and nonlinear regimes occurs at a few tenths of a calorie/cm^2 agreeing with our prediction. Also shown on this figure are the energy in a 1Ω load and the voltage developed across the enhanced region. The voltage saturates at a value corresponding to an electric field of 2.6×10^5 V/cm. As in the field limiting case, the field in the dielectric exceeds the strength of Teflon (2.4×10^5 V/cm). It is, however, not clear that dielectric breakdown strengths have any meaning when the material is highly conductive.

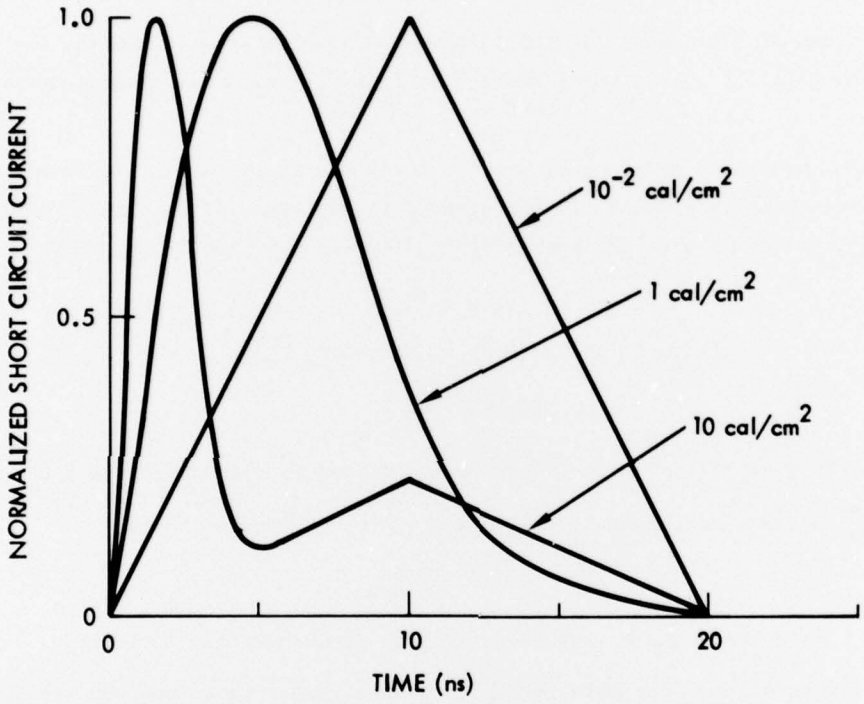

Figure 7. Comparison of Normalized Short Circuit Current Waveforms at Three Fluence Levels Showing the Effect of Transient Dielectric Conductivity.

6. LOSSY TRANSMISSION LINES

Consider a long cable which is uniformly irradiated along its length. Now it is clear for the vacuum and air gap cases that the limited driver, i.e., the short circuit current in an elemental section of cable, is coupled through the gap voltage to the solution of the rest of the cable equivalent circuit. In the absence of direct numerical techniques for the solution of the transmission line equations with nonlinear drivers, one can simulate a long cable by repeated lumped element sections in a circuit analysis code. When the cable is long compared to the distance traveled by a signal for the duration of the pulse, we will see a broadening of the load current waveform because of the staggered arrival times of current from different sections of the cable. The gap voltages, and thus the drivers, are dependent on cable length but any nonlinearity is associated with the limiting of the driver in each elemental section.

We wish to distinguish the above situation from propagation losses in the cable itself. Dielectric conductivity provides a shunt path throughout the dielectric volume which is at least as big as the conductivity due to X-ray dose rate in the bulk of the dielectric. In this situation, as the driver from one point in the cable propagates down the line, it is further dissipated in the bulk conductivity of the rest of the cable.

To illustrate propagation losses in the load response of a long cable, consider a 20 m gapless cable made of repeated sections whose equivalent circuit is analogous to that in Figure 6, along with an appropriate series inductance. The cable is terminated at both ends in a matched 50Ω load. The load response as a function of fluence will include the effects of both limiting of the driver in each section and dissipation along the length of the cable due to dielectric conductivity. The qualitative features of the response of a short 1 m cable versus the response of the 20 m cable can be seen by comparing Figures 6 and 8. The breakpoint between the linear and nonlinear regimes occurs around 0.1 cal/cm^2 for either length. Peak current and load energy in the 20 m case increase very slowly in the limited regime. Long cable response has nearly saturated compared to the comparable curves in Figure 6 which show a steady but sublinear increase in the response in the limited regime. Data are shown in Figure 8 for two treatments of the conductivity. These correspond to using the expression for conductivity given in Eq. (17) with and without the second term, i.e., delayed conductivity. Accounting for delayed conductivity does not affect the peak load current but it does decrease load energy about a factor of 5. This difference in energy is explained by the fact that with prompt conductivity only the cable returns to the lossless state at the end of the pulse; but with delayed conductivity, energy continues to be dissipated in the cable as the signal propagates to the loads after the pulse is over. Furthermore, it was only in this 20 m cable including

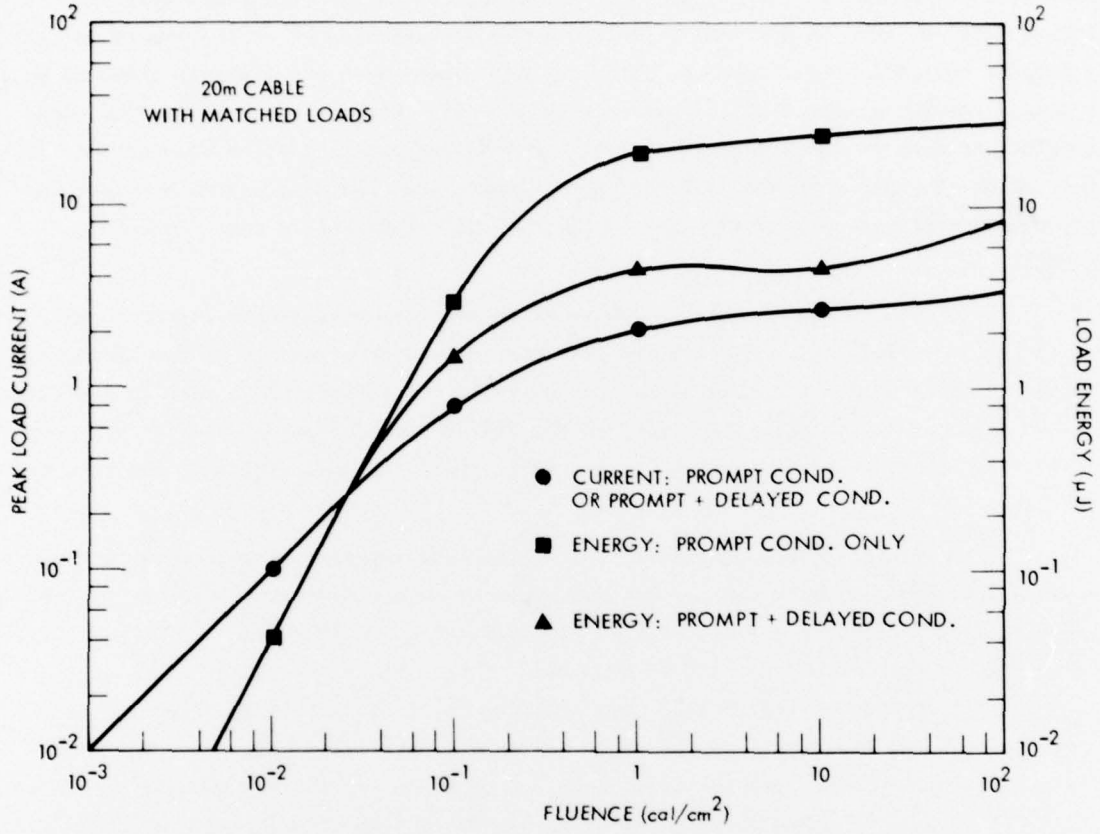

Figure 8. Load Response of a 20 m Cable as a Function of Fluence Comparing the Effect of Delayed Conductivity.

delayed conductivity where we saw a response versus fluence plot which did not increase monotonically. The slight dip in energy centered at 6 cal/cm^2 was present in our calculations. We speculate that some other choice of parameters would alter the magnitude of the dip, or eliminate it. Further study is indicated to quantify the situations under which response might decrease with increased fluence.

In Figure 9 several load current waveforms are shown. At .01 cal/cm^2 in the unlimited region, the current has the broadened shape characteristic of a propagated signal. Of course, the shape is the same with and without delayed conductivity. At 10 cal/cm^2 in the limited region, delayed conductivity almost completely attenuated current from points far away from the end of the cable. The reflection apparent in this waveform is characteristic of an open circuit at the other end of the cable. This can be explained because the shunt impedance presented by the delayed conductivity lowers the cable impedance below that of the load (50Ω). Thus, the other end looks like an open circuit.

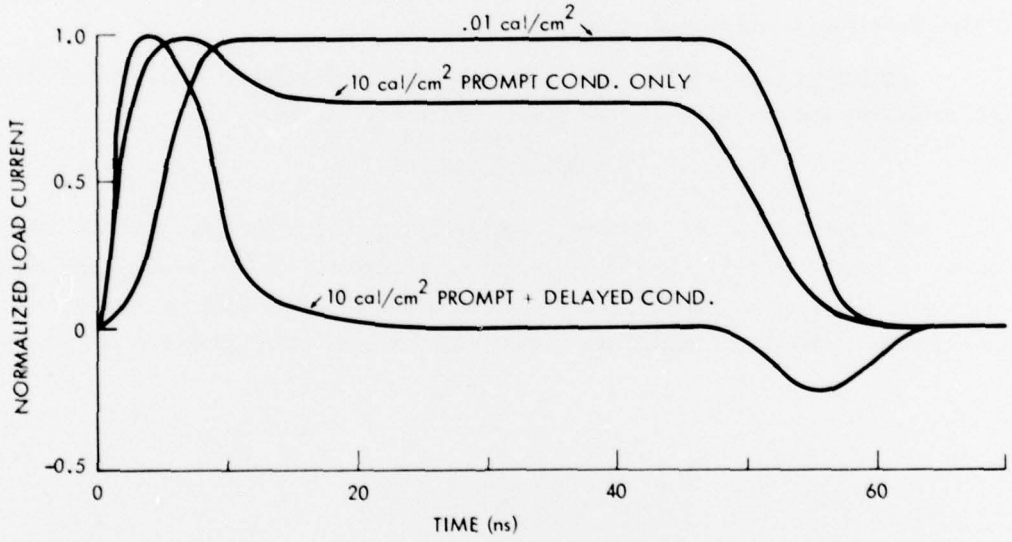

Figure 9. Comparison of Normalized Load Current Waveforms for 20 m Cable at Two Fluence Levels, Showing the Effect of Limiting by Prompt and Delayed Conductivity in the Dielectric.

7. CONCLUSIONS

We have examined three processes which can cause the X-ray induced response of a shielded cable to be nonlinear with fluence. The fluence level at which the linear region ends and the nonlinear region begins depends on details of the particular cable geometry and materials and of the X-ray environment. Estimates for the level at which limiting begins due to each process, based on results for the short circuit current per length, are as follows:

Field Limiting in Vacuum Gaps: Limiting depends on the average electron energy, the emission current per unit length per unit fluence, and the gap geometry

$$F = \frac{\bar{E}\, C_g}{eJ^p\, \Delta t} \quad (\text{cal/cm}^2) \ ;$$

Ionization in Air Filled Gaps: At one atmosphere of pressure air conductivity leads to nonlinear response at all fluences (10^{-3} cal/cm^2 is the lowest fluence at which we actually performed calculations);

Radiation-Induced Dielectric Conductivity: Limiting depends on the coefficient of prompt conductivity and the dose enhancement factor

$$D = 1/f\ K_p \ (\text{rads}) \ .$$

In addition to the limiting observed in the short circuit current, load response is further limited by the dielectric conductivity of the bulk of the cable. Propagation losses occur through this shunt as signals travel down the cable to its loads. However, delayed conductivity (when present) markedly reduces load response.

REFERENCES

1. D. M. Clement, C. E. Wuller, and E. P. Chivington, IEEE Trans. Nucl. Sci. NS-23, 1946 (1976).

2. W. L. Chadsey, B. L. Beers, V. W. Pine, and C. W. Wilson, IEEE Trans. Nucl. Sci. NS-23, 1933 (1976).

3.

4. P. R. Trybus and A. M. Chodorow, IEEE Trans. Nucl. Sci. NS-23, 1977 (1976).

5. T. A. Dellin and C. J. MacCallum, "A Handbook of Photo-Compton Current Data", Sandia Laboratories, SCL-RR-720086, December 1972.

6. R. R. Schaefer, J. Appl. Phys. 44, 152 (1973).

7.

8. C. E. Wuller, "Secondary Electron SGEMP Currents in Cable Gaps at Partial Pressures", TRW Systems Group, 99900-7810-RU-00, November 1975.

9. V. A. J. van Lint, J. W. Harrity, and T. M. Flanagan, IEEE Trans. Nucl. Sci. NS-15, 194 (1968).

10. R. C. Weingart, R. H. Barlett, R. S. Lee, and W. Hofer, IEEE Trans. Nucl. Sci. NS-19, 15 (1972).

11. W. H. Sullivan and R. L. Ewing, IEEE Trans. Nucl. Sci. NS-18, 310 (1971).

DISTRIBUTION LIST

DEPARTMENT OF DEFENSE

Director
Defense Communications Agency
ATTN: NMR

Defense Documentation Center
Cameron Station
12 cy ATTN: TC

Director
Defense Nuclear Agency
ATTN: DDST
3 cy ATTN: TITL, Tech. Library
ATTN: TISI, Archives
2 cy ATTN: RAEV

Commander, Field Command
Defense Nuclear Agency
ATTN: FCPR
ATTN: FCLMC

Director
Interservice Nuclear Weapons School
ATTN: Document Control

Chief
Livermore Division, Field Command, DNA
Lawrence Livermore Laboratory
ATTN: FCPRL

Under Secretary of Def. for Rsch. & Engrg.
ATTN: S&SS (OS)

DEPARTMENT OF THE ARMY

Director
BMD Advanced Tech. Ctr.
Huntsville Office
ATTN: RDMH-O

Dep. Chief of Staff for Rsch. Dev. & Acq.
ATTN: DAMA-CSM-N

Commander
Harry Diamond Laboratories
ATTN: DRXDO-TI, Tech. Lib.
ATTN: DRXDO-RCC, John A. Rosado
ATTN: DRXDO-RCC, Raine Gilbert
ATTN: DRXDO-NP

Commander
Picatinny Arsenal
ATTN: SMUPA
ATTN: SARPA

Commander
Redstone Scientific Information Ctr.
U.S. Army Missile Command
ATTN: Chief, Documents

Chief
U.S. Army Communications Sys. Agency
ATTN: SCCM-AD-SV, Library

DEPARTMENT OF THE ARMY (Continued)

Commander
U.S. Army Electronics Command
ATTN: DRSEL

DEPARTMENT OF THE NAVY

Chief of Naval Research
ATTN: Henry Mullaney, Code 427

Director
Naval Research Laboratory
ATTN: Code 5565, P. Ulrich
ATTN: Code 7750, Jack Davis

Officer-in-Charge
Naval Surface Weapons Center
ATTN: Code WA501, Navy Nuc. Prgms. Off.

Director
Strategic Systems Project Office
ATTN: NSP

DEPARTMENT OF THE AIR FORCE

AF Geophysics Laboratory, AFSC
ATTN: Charles Pike

AF Materials Laboratory, AFSC
ATTN: Library

AF Weapons Laboratory, AFSC
ATTN: SUL
2 cy ATTN: NTS
2 cy ATTN: DYC

Hq. USAF/RD
ATTN: RDQSM

Commander
Rome Air Development Center, AFSC
ATTN: Edward A. Burke

SAMSO/DY
ATTN: DYS

SAMSO/MN
ATTN: MNNG
ATTN: MNNH

SAMSO/SK
ATTN: SKF

SAMSO/XR
ATTN: XRS

Commander in Chief
Strategic Air Command
ATTN: XPFS
ATTN: NRI-STINFO, Library

DEPARTMENT OF ENERGY

University of California
Lawrence Livermore Laboratory
ATTN: Tech. Info. Dept. L-3

DEPARTMENT OF ENERGY (Continued)

Los Alamos Scientific Laboratory
ATTN: Doc. Con. for Reports Lib.

Sandia Laboratories
Livermore Laboratory
ATTN: Doc. Con. for Theodore A. Dellin

Sandia Laboratories
ATTN: Doc. Con. for 3141, Sandia Rpt. Coll.

OTHER GOVERNMENT AGENCY

NASA
Lewis Research Center
ATTN: N. J. Stevens
ATTN: Carolyn Purvis
ATTN: Library

DEPARTMENT OF DEFENSE CONTRACTORS

Aerospace Corporation
ATTN: Frank Hai
ATTN: V. Josephson
ATTN: Julian Reinheimer
ATTN: Library

Avco Research & Systems Group
ATTN: Research Lib. A830, Rm. 7201

The Boeing Company
ATTN: Preston Geren

University of California at San Diego
ATTN: Sherman De Forest

Computer Sciences Corporation
ATTN: Alvin T. Schiff

Dr. Eugene P. DePlomb
ATTN: Eugene P. DePlomb

Dikewood Industries, Inc.
ATTN: Tech. Lib.
ATTN: K. Lee

EG&G, Inc.
Albuquerque Division
ATTN: Technical Library

Ford Aerospace & Communications Corp.
ATTN: Donald R. McMorrow, MS G30
ATTN: Library

General Electric Company
Space Division
ATTN: Joseph C. Peden, VFSC, Rm. 4230M

General Electric Company
TEMPO-Center for Advanced Studies
ATTN: DASIAC
ATTN: William McNamara

Hughes Aircraft Company
ATTN: Tech. Lib.

Hughes Aircraft Company, El Segundo Site
ATTN: Edward C. Smith, MS A620
ATTN: William W. Scott, MS A1080

DEPARTMENT OF DEFENSE CONTRACTORS (Continued)

IRT Corporation
ATTN: Dennis Swift
ATTN: Technical Library

JAYCOR
ATTN: Library
ATTN: Eric P. Wenaas

JAYCOR
ATTN: Robert Sullivan

Johns Hopkins University
Applied Physics Laboratory
ATTN: Peter E. Partridge

Kaman Sciences Corporation
ATTN: Library
ATTN: W. Foster Rich
ATTN: Jerry I. Lubell

Lockheed Missiles & Space Co., Inc.
ATTN: Dept. 85-85

McDonnell Douglas Corporation
ATTN: Stanley Schneider

Mission Research Corporation
ATTN: Roger Stettner
ATTN: Conrad L. Longmire

Mission Research Corporation-San Diego
ATTN: V. A. J. Van Lint
ATTN: Library

R&D Associates
ATTN: Leonard Schlessinger
ATTN: Technical Library

Rockwell International Corporation
ATTN: Technical Library

Science Applications, Inc.
ATTN: William L. Chadsey

Spire Corporation
ATTN: Roger G. Little

Systems, Science and Software, Inc.
ATTN: Andrew R. Wilson
ATTN: Technical Library

TRW Defense & Space System Group
ATTN: Tech. Info. Center/S-1930
ATTN: Charles Wuller
ATTN: L. Carlisle Nielsen
ATTN: David M. Clement
2 cy ATTN: Robert M. Webb, R1-2410